N87-26018

TURBULENCE MODELING

Morris W. Rubesin
NASA Ames Research Center

ABSTRACT

Recent developments at several levels of statistical turbulence modeling applicable to aerodynamics are briefly surveyed. Emphasis is on examples of model improvements for transonic, two-dimensional flows. Experience with the development of these improved models is cited to suggest methods of accelerating the modeling process necessary to keep abreast of the rapid movement of computational fluid dynamics into the computation of complex three-dimensional flows.

NOMENCLATURE

$C_{\varepsilon 1}$ = modeling coefficient in production of dissipation rate

$C_{\varepsilon 2}$ = modeling coefficient in destruction term of dissipation rate

C_{ν} = modeling coefficient in eddy viscosity formulation

D_k = diffusion of kinetic energy

D_{ij} = diffusion of Reynolds stress, $\overline{u_i'u_j'}$

k = mean kinetic energy of turbulence

K = von Karman constant, 0.4

L = characteristic length scale

P_k = production of kinetic energy

P_{ij} = production of Reynolds stress, $\overline{u_i'u_j'}$

S_{ij} = strain rate, $\frac{1}{2}\left(\frac{\partial \bar{u}_i}{\partial x_j} + \frac{\partial \bar{u}_j}{\partial x_i}\right)$

t = time

u = velocity component in streamwise direction

U_e = velocity at boundary-layer edge

v = velocity component normal to surface

V = characteristic velocity scale

w = velocity component in transverse direction

x = coordinate in streamwise direction

$\hat{x}$ = space location vector

y = coordinate normal to surface

z = coordinate in transverse direction

β^* = modeling coefficient

δ^* = displacement thickness

δ_{ij} = Kronecker delta

ε = dissipation rate of kinetic energy

ε_{ij} = dissipation rate of Reynolds stress, $\overline{u_i'u_j'}$

ν = kinematic viscosity of fluid

ν_t = turbulent eddy viscosity

ρ = fluid density

τ_w = wall shear stress

ϕ_{ij} = pressure/rate-of-strain production of Reynolds stress, $\overline{u_i'u_j'}$

ω = specific dissipation rate, $\varepsilon/\beta^* k$

Ω_{ij} = vorticity,

$$\frac{1}{2}\left(\frac{\partial \bar{u}_i}{\partial x_j} - \frac{\partial \bar{u}_j}{\partial x_i}\right), \quad \Omega = (2\Omega_{mn}\Omega_{mn})^{1/2}$$

$()$ = mean or averaged quantity

$()'$ = turbulent fluctuating quantity

$()_i$ = vector component in ith direction, i = 1, 2, or 3

$()_{ij}$ = ijth tensor

INTRODUCTION

Numerical codes for the computation of fluid dynamical problems contain several distinct elements. These include the basic equation set, grid-generation and nesting techniques for complex configurations, efficient solution algorithms, and appropriate boundary condition treatments. In addition, if the fluid flow is turbulent, the effects of all the scales of the flow field that cannot be resolved by the numerical scheme either in time or space must be modeled. It is through this "turbulence modeling" that the numerically

unresolved physics of fluid motion is introduced into the flow-field computation.

The purpose of this paper, then, is to illustrate the current status of "turbulence modeling" as it is applied to aerodynamic flow fields, and to suggest some means of accelerating progress in its development. That the latter is particularly important was recognized by two National Academy of Sciences (NAS) groups that studied the rate of progress of computational fluid dynamics (CFD) in general and turbulence modeling in particular. In 1983, the committee headed by Robert Smelt concluded, "If the gap between progress in turbulence modeling and developments in numerical algorithms and computer hardware is allowed to continue, it could seriously impair the accuracy and usefulness of CFD towards the end of this century" (Smelt, 1983). This view was reflected again in a yet to be published 1986 National Research Council Report. As turbulence is a feature of almost every aerodynamically important flow field, this situation deserves the serious attention of the CFD community.

To examine why it is generally perceived that progress in turbulence modeling has been rather slow, it is important to understand what is involved in the creation or modification of a turbulence model. Basic to this understanding is the knowledge of the actual features of fluid turbulence and what the models can or cannot be expected to emulate.

What then is fluid turbulence? Turbulence is a fluid flow, not a fluid property. And it possesses many extremely complex characteristics. At a point in space, even when the gross flow is steady, the turbulent flow appears to be a chaotically, or randomly, unsteady event about some mean value. Over an extended space, however, some coherence can be observed in the large-scale turbulent motions under certain conditions. The turbulent flow is always three-dimensional, even when it exists within a mean motion that is one- or two-dimensional. This three-dimensionality is very important, for it provides the degrees of freedom to allow local vortices to stretch, and in so doing it transmits energy from larger-scale motions to those that are smaller. As a consequence, the turbulent flow possess an extremely large range of scales in time and space, and the range of scales between the largest, related to body dimension, and the smallest, where the turbulence dissipates quickly, increases with larger Reynolds numbers.

For an aircraft, the largest scales are a few percent of its length and carry most of the kinetic energy of the turbulence. The smallest scales, where the turbulence dissipates into heat, are about one thousandth of the local boundary-layer thickness, depending somewhat on the Reynolds number of the flow in question. Turbulence is also very diffusive and promotes mixing of sensible properties, such as temperature, chemical constituents, or momentum. For example, within aircraft engines this is a favorable property which enhances the distribution of fuel prior to combustion. On a surface of an aircraft, however, this enhanced mixing contributes to increased drag. Finally, turbulence is dissipative in that the fluid viscosity can destroy the motions of the smallest scales and convert their energy into heat. It has been observed experimentally that the large scales of turbulence are unique to individual flow situations, whereas the smaller scales tend to have a universal character. The range of scales broadens with increased Reynolds number.

Up to about 15 years ago, the limitations of available computational power forced all turbulence calculations to be confined to the use of steady-state, statistical descriptions of the turbulence. Most of the features described in the previous paragraph could not be considered in detail. Turbulence models were applied only to averaged equations, and the information contained in the real dynamical features could only be restored, approximately, through the use of empirical constants that were contained in the statistical model formulations. Then, about 15 years ago, computers were developed that had sufficient power to allow the computation of the dynamic behavior of some very simple flow fields at very low Reynolds numbers where the range of scales present is relatively small. Underlying these computations is the assumption that the Navier-Stokes equations, together with the energy-transport equation, constitute the basic equations for continuum fluid flow. It is further assumed, without rigorous mathematical proof, that these three-dimensional nonlinear equations can be solved accurately in time and space and that the solutions lie within narrow bounds despite large numbers of uncertainties that exist in defining initial and time-dependent boundary conditions.

Although these computations can capture all of the features of real turbulence described earlier, they are extremely costly and have been confined to studies of the "physics" of turbulence in idealized flow situations. These studies have resulted in descriptions of the dynamic mechanisms that take place in free and wall-bounded turbulent flows in much greater detail than can be measured in physical experiments. They also provide information on quantities that can only be measured inaccurately, if at all, for example, static pressure fluctuations or local rates of turbulence dissipation. Even though these computations deal with relatively simple flow fields of limited extent, they fill the capacity of the largest computers and require many tens of hours of computer time to reach statistically meaningful results. Some of these computations have yielded results that will be of inestimable value to the turbulence modeler, but this approach cannot be considered an engineering design tool even in the reasonably near future. The reasons for this are illustrated in figure 1.

Figure 1 compares the computer speed and memory requirements for different classes of aerodynamic computational methods with the capabilities of some large existing computers and of some that are projected for the near term (Chapman, 1978). For example, application of turbulence simulation where all the significant scales of turbulence are resolved for an airfoil (A, fig. 1) would require computer capabilities about 4 orders of magnitude larger than that labeled "Large Eddy Simulation." Clearly, such calculations cannot be considered in the foreseeable future. The regions labeled Large Eddy Simulation were estimated by Chapman under the assumption that only the sublayer regions of boundary layers need to be resolved to the small scales and that the the outer parts of the boundary layers, the regions of separation, and shedding vortices could be treated inviscidly (Chapman, 1978).

Even with the major economies afforded by these assumptions, the abilities to perform time-accurate simulations of the turbulent flow fields about aerodynamic bodies lie outside the abilities of the computers projected in the immediate future. Chapman's estimates relative to the fully resolved computational needs, however, show the importance of the development of good sub-grid turbulence models to account for turbulence scales smaller than the grids employed for the bulk of the flow. In addition, if a good sub-grid model were developed for the near-wall region of the boundary layer, the computer requirements could be reduced further from those shown, and large eddy simulations of turbulent flow about an airfoil could be anticipated in the reasonably near future, not necessarily as a design technique, but at least as a research tool. The development of good sub-grid turbulence models for large-eddy simulations, then, is a research topic that should be given considerably more emphasis than it has had in the United States. The French and the Japanese have recognized this for several years, and are well ahead of us in this research topic.

Figure 1 also illustrates that projections of computer requirements for the solution of turbulent aerodynamic flow fields about aircraft shapes with the Reynolds-averaged Navier-Stokes equations are within the capabilities of near future computers. In particular, the current NAS computer is capable of handling the turbulent flow over a complete wing with the Navier-Stokes approach and use of simple algebraic models of turbulence. It is the turbulence modeling for this class of computation that is the focus of the remainder of this paper.

STATISTICAL TURBULENCE MODELING

Reynolds-Averaged Equations

Statistical turbulence modeling begins with the derivation of the equations to represent the mean or average motions of the turbulent flow. This process can be illustrated simply by examining only the single equation representing the velocity parallel to the surface in an incompressible fluid, the instantaneous u-component equation of the Navier-Stokes system of equations:

$$\frac{\partial u}{\partial t} + u\frac{\partial u}{\partial x} + v\frac{\partial u}{\partial y} + w\frac{\partial u}{\partial z} = \frac{1}{\rho}\frac{\partial p}{\partial x} + \frac{\partial}{\partial x}\left(\nu\frac{\partial u}{\partial x}\right) + \frac{\partial}{\partial y}\left(\nu\frac{\partial u}{\partial y}\right) + \frac{\partial}{\partial z}\left(\nu\frac{\partial u}{\partial z}\right) \quad (1)$$

For a steady-state turbulent flow, the dependent variables are then expanded as the sum of their mean parts plus their turbulent fluctuations, namely,

$$u(\hat{x},t) = \bar{u}(\hat{x}) + u'(\hat{x},t) \quad (2)$$

where $\hat{x}$ represents a point in space and t is time. The overbar indicates an average quantity, and the prime represents the instantaneous fluctuation. The components of velocity v, normal to the surface, and w, in the transverse direction, are expanded similarly. Note that the steady-state requirement of this example eliminates time as an independent variable in the mean quantity.

When these velocities are introduced into equation (1), and the resulting equation is averaged over time, there results the following:

$$\bar{u}\frac{\partial \bar{u}}{\partial x} + \bar{v}\frac{\partial \bar{u}}{\partial y} + \bar{w}\frac{\partial \bar{u}}{\partial z} = \frac{1}{\rho}\frac{\partial \bar{p}}{\partial x} + \frac{\partial}{\partial x}\left(\nu\frac{\partial \bar{u}}{\partial x} - \overline{v'u'}\right) + \frac{\partial}{\partial y}\left(\nu\frac{\partial \bar{u}}{\partial y} - \overline{v'u'}\right) + \frac{\partial}{\partial z}\left(\nu\frac{\partial \bar{u}}{\partial z} - \overline{w'u'}\right) \quad (3)$$

It is noted that only the nonlinear moments of the fluctuating turbulent velocity components have survived the averaging process, which has eliminated most of the real physical details of the turbulence that were described earlier. The chaotic time dependence, the phase relationships between the turbulence velocity components, and the multitude of turbulence scales are merged into just three averaged moments of the fluctuating velocity components. The resulting equation resembles the original Navier-Stokes equation, restricted to steady flow, except for the averaged moments of velocity fluctuations that reside in positions corresponding to those of the viscous stress terms and which, consequently, are called Reynolds stresses, after their original discoverer (Reynolds, 1895).

Note that these Reynolds stresses constitute three new dependent variables, whereas no new additional equations resulted from the averaging process. Thus, more unknowns are created than

equations, and the problem is not closed, at this level, unless the Reynolds stresses can be expressed in terms of the independent variables (which are the coordinates) or the dependent variables (which are the velocity components) or both. If the six equations for the Reynolds stresses are derived from moments of the Navier-Stokes equations, it is found that these new equations contain many more than six new higher-order terms, including those that contain averages of the fluctuating velocity derivatives (Chou, 1945). The proliferation of dependent variables greatly exceeds the number of new equations derived, and this process continues as more and more equations are derived. This is called the closure problem and is the central problem of statistical turbulence theory that forces the modeling of the turbulence.

Levels of Turbulence Modeling

The turbulence models required to evaluate the Reynolds stresses in equation (3) have been expressed at a variety of levels. These will be illustrated in this section, beginning with the field equations for the Reynolds stresses. By starting with the more complex models, it can be shown that some of the simpler models follow from the imposition of certain assumptions onto the more general models.

The Reynolds-stress-transport model (RSE) can be expressed as

$$\frac{D}{Dt}\left(\overline{u_i'u_j'}\right) = P_{ij} - \varepsilon_{ij} + D_{ij} + \phi_{ij} \qquad (4)$$

The terms on the right-hand side of the equation are divided into four quantities identified with the physical processes known to occur in a turbulent flow: P_{ij} is the production of the Reynolds stress tensor; E_{ij} is the dissipation rate of the Reynolds stress tensor; D_{ij} is the diffusion of the Reynolds stress; and ϕ_{ij} is the pressure/rate-of-strain production of the Reynolds stress tensor. Of these, only the production term P_{ij} can be expressed in terms of the Reynolds stresses, the mean velocities, and the coordinates; consequently, it does not need to be modeled. The other terms are composed of third-order moments, moments of derivatives, or pressure fluctuations, all new quantities that have to be modeled. This level of modeling is called second-order closure, that is, the closure occurs in the Reynolds stress equations instead of in the Reynolds-averaged momentum equations. The equation for ε, the rate of dissipation of the turbulence kinetic energy, used to define the ε_{ij} and the length scales, requires all of its terms to be modeled. For at least two reasons, the use of second-order closure is now limited to a few practitioners: first, the addition of seven additional field equations increases computation costs by a factor of about 5 over that of the simplest models; second, the advantages that result from the use of the stress-transport equations do not justify these costs for most problems. Later in this paper, some examples will be presented for which the use of the Reynolds-stress-transport equations indicates some advantages that may merit application of these equations to certain problems.

A turbulence model that takes advantage of the inherent characteristics of the Reynolds-stress-transport equations, but only adds two field equations to the system, is called the Algebraic Stress Model (Rodi, 1976). Here the stress-transport equation is rewritten as

$$\frac{D}{D_t}\left(\overline{u_i'u_j'}\right) - D_{ij} = P_{ij} - \varepsilon_{ij} + \phi_{ij} = \frac{\overline{u_i'u_j'}}{k}\left(\frac{Dk}{Dt} - D_k\right) \qquad (5)$$

The basic assumption of the method is represented by the term on the extreme right, where it is assumed that the convection minus the diffusion of the Reynolds stresses is proportional to the same quantities in the turbulence kinetic energy equation. The Reynolds stresses can be written algebraically as

$$\frac{\overline{u_i'u_j'}}{k} = \frac{P_{ij} - \varepsilon_{ij} + \phi_{ij}}{P_k - \varepsilon} \qquad (6)$$

Recall that the production term also contains the Reynolds stresses, so that equation (6) has to be solved in an iterative manner. The kinetic energy and rates of dissipation are found from equations of the form

$$\frac{Dk}{Dt} = P_k - \varepsilon + D_k \qquad (7)$$

$$\frac{D\varepsilon}{Dt} = C_{\varepsilon 1}\frac{\varepsilon}{k}P_k - C_{\varepsilon 2}\frac{\varepsilon^2}{k} + D_\varepsilon \qquad (8)$$

The next lower level of turbulence modeling utilizes the eddy-viscosity concept, that is, the effects of turbulence are expressed in terms of an effective kinematic viscosity acting on the fluid rate of strain. The constitutive relations between stress and strain that have been utilized are shown in the following equations from Wilcox and Rubesin (1980)

$$-\overline{u_i'u_j'} = -\frac{2}{3}\delta_{ij}k + 2\nu_t\left(S_{ij} - \frac{1}{3}\frac{\partial \bar{u}_\ell}{\partial x_\ell}\delta_{ij}\right) + \frac{8/9\,k\,(S_{im}\Omega_{mj} + S_{jm}\Omega_{mi})}{(\beta^*\omega^2 + 2S_{mn}S_{mn})} \qquad (9)$$

and in that from Boussinesq (1877)

$$-\overline{u_i'u_j'} = -\frac{2}{3}\delta_{ij}k + 2\nu_t\left(S_{ij} - \frac{1}{3}\frac{\partial \bar{u}_\ell}{\partial x_\ell}\delta_{ij}\right) \qquad (10)$$

Equation (9) accounts for the effects of the interaction of vorticity and the rates of strain, which allows experimentally observed anisotropies to develop in a homogeneous shear flow. Those effects are neglected in the classic form of equation (10).

The manner of evaluating the eddy viscosity distinguishes most of the currently popular turbulence models. In general, the eddy viscosity can be written as

$$\nu = C_\nu L V \tag{11}$$

where C_ν is an empirically established coefficient or function, V is a characteristic velocity scale, and L is a characteristic length scale.

The various eddy-viscosity models are classified in Table 1; the terminology used in the table will be used in the discussion of the results to be shown later.

Table 1 Classification of eddy-viscosity models

Two-equation models:

$$V = \sqrt{k},\ L = L(k,\varepsilon)$$

One-equation models:

$$V = \sqrt{k},\ L = L(y)$$

One-half-equation models:

$$\frac{\partial}{\partial x}(\tau_{max} - \tau_{max,0}) = -C_1 (\tau_{max} - \tau_{max,0})$$

Zero-equation models:

$$V = \left(\frac{\tau_w}{\rho}\right)^{1/2}, \quad L = Ky \text{ (inner zone)}$$

$$= U_e = C_2 \delta^* \text{ (outer zone)}$$

$$\text{or } V = V(\Omega), \quad L = L[(y\Omega)_{max}]$$

The two-equation models utilize the kinetic energy and dissipation rates found from equation (7) and from forms of equation (8); thus, they require the solution of two additional field equations. This increases computer costs by about a factor of 3 over computations based on the zero-equation models shown at the bottom of the table. The reason for this increased cost is that the turbulence modeling equations are stiff; as a result, they require very small mesh dimensions near the surface when they are modified to allow their integration to the surface. It will be shown later that these cost penalties can be eliminated through the use of wall functions, that is, algebraic relationships that span the distance between the surface and the first mesh points located well into the regions where the turbulence dominates the viscous forces.

Particular attention should be given to the model in Table 1 designated as a one-half-equation model. The "one-half" is used to emphasize the fact that an ordinary differential equation is added to the Reynolds-averaged Navier-Stokes system instead of another partial differential field equation. In the example shown here, the subscript 0 under the shear-stress symbol means an equilibrium value or one given by the zero-equation models indicated on the lower portion of the table. The subscript max means the maximum shear stress at some point within the boundary layer at the station, x. Thus, the one-half-equation model accounts for the lag in the development of the turbulence that occurs when the mean motion is modified by the imposition of a large streamwise pressure gradient. The dependent variable, the maximum shear stress in this case, is then used to scale the turbulence algebraically across the entire viscous region at station x.

The zero-equation models (Table 1) represent the eddy viscosity in two zones, or layers, of the viscous region. Near the surface, the velocity scale usually used is the local friction velocity, $\sqrt{\tau_w/\rho}$, and the length scale is merely proportional to the distance from the surface. In the outer zone, the velocity scale is the velocity at the edge of the viscous region and the scale depends on the displacement thickness (Cebeci and Smith, 1974). In those situations where it is difficult to define these terms, that is, where the inviscid region has a non-uniform velocity field, the velocity and length scales have been expressed in terms of the local vorticity that occurs where the moment of vorticity is a maximum (Baldwin and Lomax, 1978). Since all of these quantities are expressible algebraically in either the dependent or independent variables of the mean-flow equations, no additional partial differential equations for field variables are required and these are termed zero-equation models.

Difficulties in Applying and Developing Turbulence Models

In a particular application, the level of turbulence model that can be considered must reflect the computational power available and the solution algorithms to be used. Limited computational power permits only the simplest of turbulence models to be considered. Also, the turbulence model employed has a strong influence on the numerical behavior of the algorithms. Not all algorithms that can solve laminar flows can be applied to turbulence models, especially those that use field equations for turbulence quantities such as the Reynolds stresses, kinetic energy, or dissipation rate. Iteration processes are influenced considerably by the stiffness of the turbulence field equations. Also, algorithms that require conservative forms have difficulty with

the source and sink terms that are inherent in the turbulence field equations to reflect the turbulence production and dissipation that occur within the real turbulent flow. Finally, the turbulence models also impose constraints on the usable mesh configurations by requiring very close spacings between meshes in the vicinity of surfaces.

This strong influence of the turbulence model on the numerical scheme has made it difficult to assess the quality of particular turbulence models, because often a significant part of the disagreement between computed results and experimental data is numerical, resulting from a previously verified algorithm's difficulty with the constraints introduced by a new turbulence model. Once these numerical difficulties are overcome and the turbulence models can be applied with confidence, the resulting disagreement with experimental data for a particular flow field can be ascribed to the limitations of a the particular turbulence model being employed. At this point, provided fundamental experimental turbulence data are available to guide its improvement, it is possible to remodel the turbulence model to improve its performance for the complex flow in question, and to do so in a manner that does not alter its behavior for simpler flow fields for which it had already proved successful. Some examples of this process are shown in the following section where the state of the art of statistical turbulence modeling is summarized with a few selected flow conditions.

APPLICATION OF VARIOUS LEVELS OF TURBULENCE MODELING

In this section, in order to provide a brief overview of the state of the art of turbulence modeling, various levels of turbulence modeling will be applied to a variety of flow fields of interest to aerodynamics. Both original models and the consequence of "remodeling" will be shown in several examples. Care has been taken in most of these calculations to eliminate numerical uncertainties, so that any differences shown between the computed results and experimental data can be ascribed to turbulence-model deficiencies.

The first flow to be considered deals with the effect of large streamwise pressure variations on the skin friction of an attached turbulent boundary layer (Kussoy et al., 1978). In figure 2, a sketch is shown of the experimental arrangement. The boundary layer being measured was formed on the inside surface of a tube downstream from a supersonic nozzle creating an axisymmetric flow at $M = 2.3$. The pressure distribution impressed upon the boundary layer was created by a center body that compressed and then expanded the flow. The resulting pressure distribution, normalized by the upstream wall pressure where $M = 2.3$, is shown in the upper left corner of this figure. In this example, the pressure rise almost doubles its original value before relaxing. This nondimensional pressure distribution remained essentially fixed as the wind-tunnel pressure was altered to obtain a large range of Reynolds numbers. The skin friction was measured with a buried wire gauge (Rubesin et al., 1975). The skin-friction distribution was achieved with a fixed skin-friction gauge by moving the centerbody upstream and downstream about 20 cm along its axis. This provides about the same distribution of skin friction that would be achieved with a fixed centerbody and a moving skin-friction gauge, because the boundary layer ahead of the pressure rise was close to uniform thickness.

Measured and calculated skin-friction distributions are shown in figure 2 for four values of Reynolds number. Five levels of turbulence modeling are shown: a zero-equation model by Cebeci and Smith (1974) in its original form and as subsequently "remodeled" to account better for streamwise pressure gradients (Cebeci and Smith, 1974); a two-equation model by Wilcox and Rubesin (1980); and two stress-transport models. One of the stress-transport models utilizes a length scale that is prescribed algebraically (Sullivan, 1976), whereas the other uses a field equation for specific dissipation to create a length scale (Wilcox and Rubesin, 1980).

With the exception of the original zero-equation model at the lowest Reynolds number, which tends to separate prematurely, all the models show similar variations relative to the experimental data. The computed results drift through the data with increases in the Reynolds number. Computed results that are low at the lower Reynolds numbers tend to be high when the Reynolds numbers are high. No one model is clearly superior to the others over the entire Reynolds-number range, though they do seem to maintain their relative positions to each other. One can conclude from this work that for an attached boundary layer there is little advantage to using the more complex models, but if it were necessary to know the skin friction in attached boundary layers in strong streamwise pressure gradients to a few percent, improvements to all the levels of models would be required.

Streamwise curvature of a surface has a pronounced effect on the behavior of a boundary layer flowing over it (Bradshaw, 1973). This is demonstrated in figure 3, where skin friction and shape-factor data obtained on a convex surface in an adverse pressure are shown (So and Mellor, 1972). The data are expressed in terms of the streamwise distribution of the skin-friction coefficient and the shape factor of the turbulent boundary layer flow. Also shown in the figure are the computed results utilizing four turbulence models (Wilcox and Rubesin, 1980). The dashed and dot-dashed curves are based on a two-equation and a Reynolds-stress transport model in which the effects of curvature have been neglected. These

skin-friction coefficient curves depart considerably from the experimental data. The shape factor on a flat plate would remain at a value of about 1.4, again showing curvature effects that are large in affecting the boundary-layer velocity profiles. The solid and dotted curves represent the same models modified to account for the surface curvature through the introduction of a curved coordinate system. The modification to the two-equation model also required the introduction of a new centrifugal force term in the turbulent kinetic energy equation; that term vanishes on a flat surface. This was done in a rather ad hoc manner, utilizing some guidance from the the form of the Reynolds-stress equation for $\overline{v'v'}$. On the other hand, no physical modifications were made in the Reynolds-stress model. In both of these models, the specific rate-of-dissipation equation used to define the length scale was not altered except for the coordinate modifications. Figure 3 shows that the effects of the streamwise curvature in these data are represented very well by these latter computations.

It is very significant that no modifications had to be made to the Reynolds-stress turbulence model to allow it to capture the effects of streamwise curvature; it is thereby an example in which, at least in principle, the more complex form of modeling has a fundamental advantage. Another conclusion, however, is that the simpler two-equation model can also be "remodeled" to give good results on a convex surface, without altering its behavior, for cases in which the streamwise curvature is absent. A cautionary note is in order here: concave surfaces may not be calculated well with any of these models because the models completely ignore the possibility of the existence of Gortler vortices that are present over such surfaces and that can enhance the transport within the boundary layer.

Figure 4 shows the experimental data and computed results for the distribution of surface pressure and skin friction in the vicinity of a normal shock wave in an $M = 1.48$ airstream. These measurements were obtained on the inner surface of a circular tube with a static pressure tap and a flush hot-wire skin friction gage (Mateer et al., 1976). The shock-wave position could be moved relative to the fixed gauges by increasing or decreasing the blockage of a downstream shock generator.

The experimental data are compared with computations utilizing four different turbulence models: 1) two-equation models from Wilcox and Rubesin (1980), Jones and Launder (1972), and Chien (1982); and 2) a zero-equation model from Cebeci and Smith (1974), which did not incorporate the pressure-gradient modification discussed in connection with figure 2. All of these models were used in computations that extended to the surface. It should be noted that each of the models performs quite well on a flat plate at uniform pressure. The models of Jones and Launder and of Chien are very similar, except that the latter was more closely fitted to experimental channel data.

When these models are applied to the shock-wave and boundary-layer interaction of this experiment, it is found that all of them yield excellent surface-pressure distributions. The skin-friction results, however, are far from satisfactory for all but the Wilcox-Rubesin model. The Chien model, which behaves so well on a flat plate, yields surprisingly poor results in the vicinity of the shock wave. The Jones-Launder and Cebeci-Smith models fail to agree, in opposite ways, with the skin friction, the latter model indicating an extensive region of separation where none existed experimentally.

Qualitatively, this behavior is consistent with the behavior of the Cebeci-Smith model in figure 2, when it was not altered to account for pressure gradients. From a comparison of the different skin-friction results based on the different two-equation models, it can be concluded that models at the same level that are "calibrated" with flat-plate data can behave much differently when applied to a complex flow. This suggests that in general, the predictability of any turbulence model should be suspect until it is verified for a variety of complex flows.

In an effort to determine why the Jones and Launder and the Chien turbulence models predicted such different skin-friction results, Viegas and Rubesin (1983) eliminated the near-surface modeling in these turbulence models by applying the concept of wall functions to the computations shown in figure 4. This concept requires the first mesh point off the surface to lie well within the fully turbulent flow and therefore connect the flow at this point to the surface conditions with algebraic formulas. For example, a wall function in its simplest form is the conventional "law of the wall" applied to a zero-equation turbulence model on a flat plate with small streamwise pressure gradients. The two-equation models require more complex wall functions that account for the growth of turbulence kinetic energy in regions of strong pressure gradients, the mean values of kinetic energy and dissipation rates within the first mesh volume off the surface, and the changes to the law of the wall caused by local pressure gradients.

Figure 5 shows the results of applying such wall functions to the test conditions described in figure 4. Again, the surface pressure is well predicted when the different models use wall functions at distances from the wall shown by the corresponding upstream values of $y+$ indicated in the figure. The skin friction results show clearly that it is the individual near-wall treatments of the two-equation models by Jones and Launder and by Chien that causes their anomalous behavior shown in figure 4.

With wall functions, the results given by the two models are essentially identical and quite consistent with the other two-equation model by Wilcox and Rubesin. The Cebeci-Smith model with its wall function is quite consistent with the earlier results where it was computed to the surface, except in the immediate region of the separation zone where the pressure gradients are sufficiently high to bring into question the use of a usual law of the wall. It is gratifying that the wall functions not only collapse the results of the different two-equation models, but that results agree quite well with the experimental skin-friction data. Another significant bonus of the use of wall functions is that the costs of the computations were reduced by a factor of 8 because of the reduced number of mesh points needed to resolve the near-wall region and the elimination of much of the stiffness of the turbulence modeling equations. In this case, accuracy and economy were achieved together.

Figure 6 shows the results of improvements to two different levels of turbulence models applied to the computation of a shock-wave and boundary-layer interaction in transonic flow. The experimental data used in this comparison are from Johnson et al. (1982) and they were measured on an axisymmetric circular-arc bump indicated schematically in figure 6. The free-stream Mach number of the examples shown here is $M = 0.876$ and the unit Reynolds number is 13.1×10^6/m.

The upper part of figure 6 shows the distributions of surface pressure measured in the experiment and computed from four turbulent models. The abscissa begins at mid-chord of the bump and continues about a half-chord downstream after its trailing edge. The lower part of the figure shows the distribution of skin friction from two of the computations and the experimental points of separation and attachment, as they were indicated by an oil-film technique. This demonstrates that there was a rather extensive region of separated flow in this experiment.

The computed surface pressures based on the zero-equation turbulence model of Cebeci and Smith (1974) are represented by the dashed line. These results indicate that this model predicts a shock-wave position that is well downstream of its measured location. The computations also show much higher pressure in the region of separation than do the data. The dotted line represents the computed results obtained with the half-equation model of Johnson and King (1985). The latter model accounts for the history of the development of maximum shear stress in the streamwise direction through the use of an ordinary differential equation. This maximum shear stress is then used to scale an algebraic model, similar to that of Cebeci and Smith, at each station. Although these experimental data, for a range of Mach and Reynolds numbers, were used to evaluate the lag constants used in this model, the resulting agreement of the computed results with the shape of the entire pressure distribution for this particular case is remarkable. Without altering the modeling coefficients, good results have been obtained by Johnson and King in comparisons with other two-dimensional data under widely different flow conditions (Simpson et al., 1981). In addition, this model is economical to use, for it requires very little more computer time than do the standard zero-equation models.

When a two-equation model is applied to this flow, the dot-dashed line (fig. 6) results for the predicted pressure distribution. Although it performs better than the zero-equation model, the pressure distribution calculated with the two-equation model also shows a shock-wave location that is downstream of the experimental position, and the pressure is overpredicted to some extent in the region of separation. When improved wall functions (Viegas et al., 1985; Rubesin and Viegas, 1985) are applied to this Jones-Launder model, the calculated pressure distribution is considerably improved, giving results equivalent to the Johnson-King model except at the upstream foot of the shock wave. It should be noted that the forms of the wall functions or the original model were not altered to fit these particular pressure data. The use of wall functions with the Jones-Launder model also improves the prediction of the location of separation and reattachment as is seen in the skin-friction coefficient figure.

In conclusion, figure 6 shows that two turbulence models are available that can give good surface-pressure distribution results in a transonic flow over an airfoil-like body. For two-dimensional flows with a closed separation region, the model of choice is the Johnson-King model for accuracy and economy of application. It is not clear at present, however, how or if this model can be extended to three-dimensional flows. The two-equation model is directly extendable to three dimensions; however, it requires some additional modeling regarding the degree of isotropy of the eddy viscosity, and the wall-function approach in its present form is constrained to no skewing of the mean-velocity vector within the first mesh volume off the surface.

Figure 7 shows the results of applying several levels of turbulence modeling (Coakley, 1986) to the prediction of the lift and drag of an RAE 2822 airfoil for three test Mach numbers and angles of attack (Cook et al., 1979). The computations are shown here in lift-drag form to allow comparison of the results relative to a constant lift-drag ratio as shown by the lines passing through the three starred data points. Coakley (1986) used six different turbulence models: two zero-equation models, that of Cebeci and Smith and of Baldwin and Lomax; the Johnson-King half-equation model; and three versions of the two-equation model, Chien's and two originated by Coakley. The symbols used for the results found from these models are indicated on the figure.

The comparison of the experimental data and the computed results can be observed from two points of view. First, a small vector distance between the experimental and computed points reflects good agreement between the experimental data and computation for both 1) surface-pressure distributions and shock-wave locations, and 2) skin-friction distributions. Second, the alignment with the constant L/D line suggests that a particular model can yield a result that happens to provide good L/D, although in reality it misses the details.

The cases represented by the three Mach numbers correspond, with increasing Mach number, to unseparated subcritical flow, unseparated supercritical flow, and separated supercritical flow, respectively. Except for two cases at $M = 0.73$, the computed results yield values of lift and drag that are higher than the measurements. At all three Mach numbers, the Johnson-King model lies closest to the data, even at the severest flow with separation. The other models generally become poorer as the flow becomes more complex. The q-ω2 model of Coakley, while second-best overall in agreeing with the experimental results, yields a much poorer lift-drag slope than do the other models when separation takes place.

The earlier conclusion that the Johnson-King model is the model of choice for two-dimensional transonic flows is further supported by these data. For those interested only in the ratio of lift to drag, the simplest models of Cebeci-Smith and Baldwin-Lomax are reasonably adequate. These conclusions, however, are subject to the caveat that these data resulted from flows that were entirely attached or flows that separated and then reattached on the airfoil. Cases with massive separation may favor other turbulence models.

The next few figures will show the performance of various turbulence models for three-dimensional flows. Although the first two examples are strictly two-dimensional from a mathematical viewpoint, that is, axisymmetric flow or flow over an infinitely long, swept-back airfoil, the flows exhibit the skewing of the velocity vector parallel to the surface that is characteristic of three-dimensional boundary-layer flows.

Figure 8 describes skin-friction results obtained on the surface of a circular cylinder whose axis was mounted colinear with that of a low-speed wind tunnel (Higuchi and Rubesin, 1981; Driver and Hebbar, 1985). The particular feature of this experiment was that the cylinder was segmented so that a central portion of the cylinder could be rotated to introduce a shear-driven cross flow (see sketch in fig. 8). In the stationary region ahead of the rotating segment, the boundary layer develops the four Reynolds stresses, $\overline{u'u'}$, $\overline{v'v'}$, $\overline{w'w'}$, and $\overline{u'v'}$, which are characteristic of two-dimensional flow. Over the spinning portion, the additional Reynolds stresses, $\overline{u'w'}$ and $\overline{v'w'}$, are activated, and it is the latter stress that causes the mean-velocity vector to skew in a three-dimensional boundary layer. In the experiment, the relaxation of the Reynolds stresses back to their two-dimensional character is studied on the downstream stationary cylinder.

Figure 8 shows the development of the axial and cross-flow skin friction with distance along the stationary downstream cylinder. The experimental data were measured with a variety of techniques: buried hot-wire gauges, surface fences (Higuchi, 1983), and momentum integral balances. Computed results based on three levels of turbulence modeling are also shown. These include the zero-equation Aquilar (1976) model which is an extension to three dimensions of the Cebeci-Smith model, and the two-equation and Reynolds-stress-transport models of Wilcox and Rubesin. Note that both the zero-equation and the two-equation models utilize the additional assumption that the eddy viscosity is a scalar quantity that acts equally on the axial and cross-flow strains. Generally, all the models capture the behavior of the relaxation of the skin friction in both directions. Of the three models, however, the Reynolds-stress-transport model yields the best agreement with the data, except for the short region at the beginning of the stationary cylinder where the relaxation process is occurring very rapidly. Since this flow remains attached, it is believed the shortcomings of the zero-equation and two-equation models, both of which are eddy-viscosity models, are caused by the the scalar eddy-viscosity assumptions and not by problems of length scale.

Figure 9 shows oil-film streaks on the surface of flow over a transonic wing, swept back at an angle of 32° in an airstream at $M = 0.74$ and $Rec = 4.7 \times 10^6$ (Mateer and Brosh, 1983). The airfoil shape is a NACA 0012 at zero angle of attack. The wing spans the wind tunnel, but the experiment is unique in that the side walls of the wind tunnel were contoured to follow the expected inviscid flow, thereby causing the model to behave as one of infinite length where surface pressures are essentially uniform in the spanwise direction. Also shown on the figure are the surface streamlines as computed by three levels of models. Line 1 refers to a Reynolds-stress-transport model; line 2 to a two-equation model; and lines 3 and 4 refer to a mixing-length model. These models are identical to those shown in the previous figure for the spinning cylinder experiment.

Two results for the mixing-length model are shown to demonstrate the influence of the location of transition, which can be specified in this turbulence model. In the other models the location of transition is established by stability criteria built into the models. The mixing-length model shows an increased deviation from the oil-flow data as transition is moved downstream. As with the spinning cylinder, the Reynolds-stress-transport model gives slightly better results as

represented by the oil-flow pattern near the suction peak.

Figure 10 also shows a comparison of experimental and computed surface skin-friction lines for a three-dimensional flow (Horstman et al., 1985). In this case, the test body consists of a cylinder followed by skewed flare. The airstream conditions are $M = 3$ and the length Reynolds number of the boundary layer just upstream of the flare is 18×10^6. The flare is a 60° total-angle cone tilted to an angle of attack of 23°. The computations for this flow were based on the Jones-Launder two-equation turbulence model with boundary conditions supplied by wall functions (Viegas and Rubesin, 1983). The use of wall functions was critical to reduce the cost of these computations.

The oil-flow lines on the left of this figure show that for these conditions the shock wave generated by the flare is sufficiently strong to cause the boundary layer on the cylinder to separate well upstream of the cylinder-flare junction and to reattach about halfway up the flare. Considerable amounts of turning of the near-surface flow takes place within this separation zone and in the immediate region after reattachment. The computed surface shear lines show the general character of measured oil streaks; however, the details are off to quite an extent. The computed upstream separation location is only about one-half its experimental distance from the flare junction. The poor behavior of the computations is also reflected in a generally smaller upstream movement in the computed results in the vicinity of the flare. Although the reattachment region is predicted fairly well, the flow direction on the cylinder downstream of the flare also departs from the experimental data.

How these differences are felt quantitatively is shown in a comparison of the computations with the experimentally measured surface pressures in figure 11, where the surface pressures on the windward ray are plotted along the cylinder, flare, and afterbody. The smaller predicted separation zone is again evident in this figure. These quantitative results of the computations show the position of the maximum pressure to be a bit upstream of the measured location and to yield a smaller value than measured. These results suggest that the computed side force and pressure drag are low. Recently, Brown et al. (1987) made measurements of mean flow and the Reynolds stresses under these same flow conditions. These data have not yet been analyzed with the view of improving the turbulence modeling; however, this activity is under way and should lead to a remodeling of the turbulence model that will result in computations that are considerably improved over those shown here.

CONCLUDING REMARKS

Certain observations can be drawn from this brief survey of recent developments in statistical turbulence modeling applicable to aerodynamics. For attached boundary layers upstream of pressure gradients, all levels of turbulence modeling give about the same results. This is not surprising because the attached flat-plate boundary layer has been used universally to "calibrate" these models. Under severe pressure gradients, however, many popular models still yield results that differ from experimental skin-friction data by as much as 40% when the Reynolds numbers are about 100×10^6 or larger. This is a turbulence modeling topic that requires additional attention.

The manner of modeling streamwise curvature effects is also still an open question. The simplest zero-equation models use an ad hoc correction method recommended by Bradshaw (1973). On a convex surface, the two-equation models account for curvature by either increasing the rate of production of dissipation (Ha and Lakshminarayana, 1980), by diminishing the rate of destruction of dissipation (Launder et al., 1977), or by letting the dissipation rate alone and altering the rate of production of kinetic energy by introducing the work of centrifugal forces (Wilcox and Rubesin, 1980; Pulliam et al. 1985). The full Reynolds-transport model, on the other hand, requires no changes other than the introduction of curved coordinates (Wilcox and Rubesin, 1980). This variety of approaches for the introduction of the effects of surface curvature into the zero- and two-equation turbulence models illustrates the fact that these models are merely such gross approximations to the physical turbulence that there is no unique way of modeling a particular phenomenon. Consequently, a model can only be gauged by its success or failure in its application to a particular flow field or to a range of flow fields. There is no a priori way of assessing the accuracy and breadth of application of turbulence models other than by comparison with experimental data. From such comparisons, it is generally observed that the higher levels of turbulence models tend to have broader ranges of application, but that for a given application they are likely to be less accurate than simpler models that have been fitted to the particular application. The simple, or low-level, models, though computationally economical, need a data base for every class of flow likely to be encountered, and their use places an enormous burden on the numbers of experiments required. Without such a data base, the simple models are not much sounder than intelligent guesses. It is this burden on experiment that stimulates the search for more general models that are sufficiently accurate for a variety of applications even though they may cost more to compute. The user must gauge these trade-offs in deciding which models he will employ.

With respect to the rate of progress in turbulence modeling, the development of the Johnson-King model is a good example. From the time of the first experiment on airfoils in which Johnson was measuring turbulence quantities (Johnson and Bachalo, 1980) to the recent successful tests of the model he and a colleague developed (Johnson and King, 1985), 6 years elapsed. Much of this time was spent by Johnson in analyzing his data with a variety of borrowed computer codes, some of which were in development and were extremely difficult and time-consuming to operate. During this period, he also performed an additional experiment on the axisymmetric bump model that was used to complement the original airfoil data. This short history demonstrates that turbulence modeling is composed of a variety of activities that encompass analysis of the modeling equations, experimentation, the use of and modification of complex computer codes, and, most important, a dedication to do the necessary labor to improve an existing model.

When one or two individuals attempt this, the level of effort required is bound to take considerable elapsed time. Something as relatively direct as developing wall functions for compressible flows, utilizing the experimental work of others and making small modifications to existing computer codes (Viegas and Rubesin, 1983; Viegas et al., 1985), took a little longer than 2 years. Because of its dependence on a variety of disciplines, turbulence modeling is a slow process and its development can be accelerated only by an increased level of the coordinated efforts of dedicated people possessing a variety of complementary talents in analysis, experimentation, and computational-code development. This is especially required now as the CFD community begins to emphasize complex three-dimensional flow fields and requires improved turbulence models for such flows.

REFERENCES

Aquilar, F.: A Numerical Analysis of Turbulent Flow along an Abruptly Rotated Cylinder. Ph.D. Thesis, Virginia Polytechnic Institute and State University, Blacksburg, Va., 1976.

Baldwin, B. S.; and Lomax, H.: Thin-Layer Approximation and Algebraic Model for Separated Turbulent Flows. AIAA Paper 78-257, Jan. 1978.

Bradshaw, P.: Effects of Streamline Curvature on Turbulent Flow. AGARD-AG-169, 1973.

Brown, J. D.; Brown, J. L.; Kussoy, M. I.; Horstman, C. C.; and Holt, M.: Two-Component LDV Investigation of 3-Dimensional Shock/ Turbulent Boundary Layer Interactions. AIAA Paper 87-0553, Reno, Nev., 1987.

Cebeci, T.; and Smith, A. M. O.: Analysis of Turbulent Boundary Layers. Academic Press, 1974.

Chapman, D. R.: Computational Aerodynamics Development and Outlook. AIAA Journal, Vol. 17, No. 12, 1978.

Chien, K. Y.: Predictions of Channel and Boundary Layer Flows with a Low-Reynolds-Number Turbulence Model. AIAA Journal Vol. 20, Jan. 1982, pp. 33-38.

Chou, P. Y.: On Velocity Correlations and the Solutions of the Equations of Turbulent Fluctuation. Quarterly of Applied Mathematics Vol. 3, 1945, pp. 38-54.

Coakley, T. J.: Impact of Turbulence Modeling on Numerical Accuracy and Efficiency of Compressible Flow Simulations. NASA TM-88333, 1986.

Cook, P. H.; McDonald, M. A.; and Firmin, M. C. P.: Aerofoil RAE 2822 Pressure Distributions, and Boundary Layer and Wake Measurements. AGARD Advisory Report No. 138, 1979.

Driver, D. M.; and Hebbar, S. K.: Experimental Study of a Three-Dimensional, Shear-Driven, Turbulent Boundary Layer Using a Three-Dimensional Laser Doppler Velocimeter. AIAA Paper 85-1610, Cincinnati, Ohio, 1985.

Ha, C.; and Lakshminarayana, B.: Prediction of Two-and Three-Dimensional Asymmetrical Turbulent Wakes, Including Curvature and Rotation Effects. AIAA Journal, Vol. 18, Oct. 1980, pp. 1196-1204.

Higuchi, H.: A Miniature Directional Surface-Fence Gage for Three-Dimensional Turbulent Boundary Layer Measurements. AIAA Paper 83-1722, Danvers, Mass., 1983.

Higuchi, H.; and Rubesin, M. W.: An Experimental and Computational Investigation of the Transport of Reynolds Stress in an Axisymmetric Swirling Boundary Layer. AIAA Paper 81-0416, St. Louis, Mo., 1981.

Horstman, C. C.; Kussoy, M. I.; and Lockman, W. K.: Computation of Three-Dimensional Shock-Wave/Turbulent Boundary-Layer Interaction Flows. Third Symposium on Numerical and Physical Aspects of Aerodynamic Flows, California State University, Long Beach, Calif., Jan. 1985.

Johnson, D. A.; and Bachalo, W. D.: Transonic Flow past a Symmetrical Airfoil--Inviscid and Turbulent Flow Properties. AIAA Journal, Vol. 18, Jan. 1980, pp. 16-24.

Johnson, D. A.; Horstman, C. C.; and Bachalo, W. D.: Comparison between Experiment and Prediction for a Transonic Turbulent Separated Flow. AIAA Journal, Vol. 20, June 1982, pp. 737-744.

Johnson, D. A.; and King, L. S.: A Mathematically Simple Turbulence Closure Model for Attached and Separated Turbulent Boundary Layers. AIAA Journal, Vol. 23, Nov. 1985, pp. 1684-1692.

Jones, W. P.; and Launder, B. E.: The Prediction of Laminarization with a Two-Equation Model of Turbulence. International Developments in Heat Transfer, Vol. 15, 1972, pp. 303-314.

Kussoy, M. I.; Horstman, C. C.; and Acharya, M.: An Experimental Documentation of Pressure Gradient and Reynolds Number Effects on Compressible Turbulent Boundary Layers. NASA TM-78488, 1978.

Launder, B. E.; Priddin, C. H.; and Sharma, B. I.: The Calculation of Turbulent Boundary Layers on Spinning and Curved Surfaces. ASME Journal, Vol. 5, July 1967, pp. 1231-1237.

Mateer, G. G.; and Brosh, A.: Contouring Tunnel Walls to Achieve Free-Air Flow over a Transonic Swept Wing. AIAA Paper 83-1725, Danvers, Mass., 1983.

Mateer, G. G.; Brosh, A.; and Viegas, J. R.: A Normal Shock-Wave Turbulent Boundary Layer Interaction at Transonic Speeds. AIAA Paper 76-161, 1976.

Pulliam, T. H.; Jesperson, D. C.; and Barth, T. J.: Navier-Stokes Computations for Circulation Controlled Airfoils. AIAA Paper 85-1587, Cincinatti, Ohio, 1985.

Reynolds, O.: On the Dynamical Theory of Incompressible Viscous Fluids and the Determination of the Criterion. Philosophical Transactions of the Royal Society of London, Series A, Mathematical and Physical Sciences, Vol. 186, No. 123, 1895.

Rodi, W.: A New Algebraic Relation for Calculating the Reynolds Stresses. ZAMM, Vol. 56, 1976, pp. 219-221.

Rubesin, M. W.; Okuno, A. F.; Mateer, G. G.; and Brosh, A.: Flush-Mounted Hot-Wire Gage for Skin Friction and Separation Detection Measurements. Sixth International Congress on Instrumentation in Aerospace Simulation Facilities, Ottawa, Canada, Sept. 1975.

Rubesin, M. W.; and Viegas, J. R.: A Critical Examination of the Use of Wall Functions as Boundary Conditions in Aerodynamic Calculations. Third Symposium on Numerical and Physical Aspects of Aerodynamic Flows, California State University, Long Beach, Calif., Jan. 1985.

Smelt, R.: The Influence of Computational Fluid Dynamics on Experimental Aerospace Facilities, A Fifteen Year Projection. National Academy Press, Washington, D. C., 1983.

Simpson, R. L.; Chew, Y.-T.; and Shivaprasad, B. G.: The Structure of a Separating Turbulent Boundary Layer. Part. 1. Mean Flow and Reynolds Stresses. Journal of Fluid Mechanics, Vol. 113, 1981, pp. 23-51.

So, R. M. C.; and Mellor, G. L.: An Experimental Investigation of Turbulent Boundary Layers along Curved Surfaces. NASA CR-1940, 1972.

Sullivan, R. D.: GYC: A Program to Compute the Turbulent Boundary Layer on a Rotating Cone. Aeronautical Research Associates of Princeton, Working Paper No. 76-2, Aug. 1976.

Viegas, J. R.; and Rubesin, M. W.: Wall-Function Boundary Conditions in the Solution of the Navier-Stokes Equations for Complex Compressible Flows. AIAA Paper 83-1694, Danvers, Mass., 1983.

Viegas, J. R.; Rubesin, M. W.; and Horstman, C. C.: On the Use of Wall Functions as Boundary Conditions for Two-Dimensional Separated Compressible Flows. AIAA Paper 85-0180, Reno, Nev. 1985.

Wilcox, D. C.; and Rubesin, M. W.: Progress in Turbulence Modeling for Complex Flow Fields Including Effects of Compressibility. NASA TP-1517, 1980.

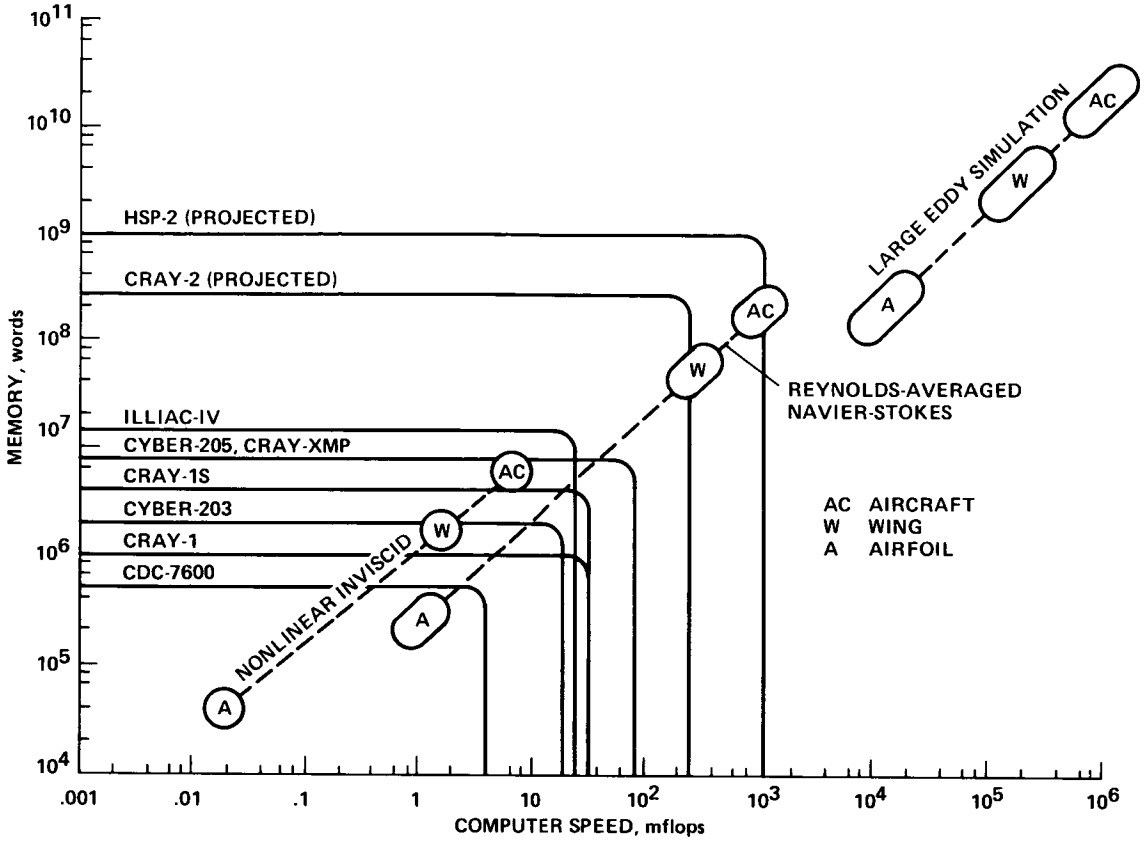

Fig. 1 Computer speeds and memory requirements for various classes of turbulence computations-based on 15 min runs with 1985 algorithms.

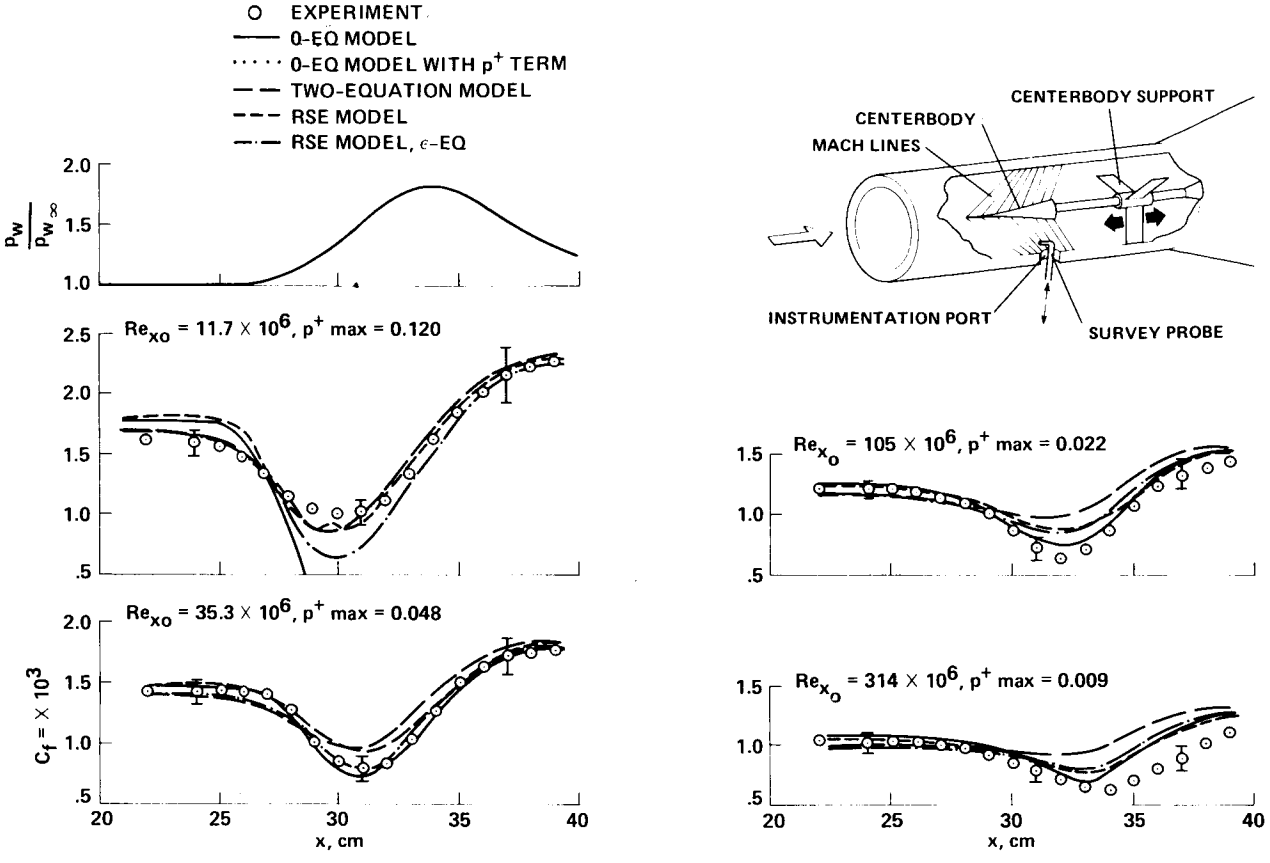

Fig. 2 Compressible boundary layer skin friction in an axial pressure gradient.

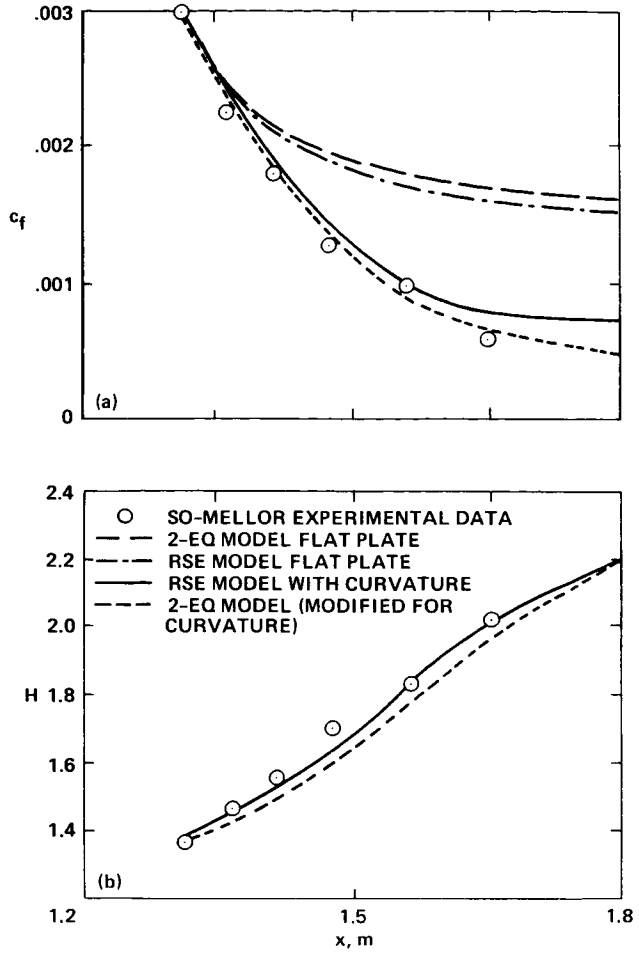

Fig. 3 Boundary layer development on a convex surface in a low speed flow with an axial pressure gradient. (a) Skin friction; (b) shape factor.

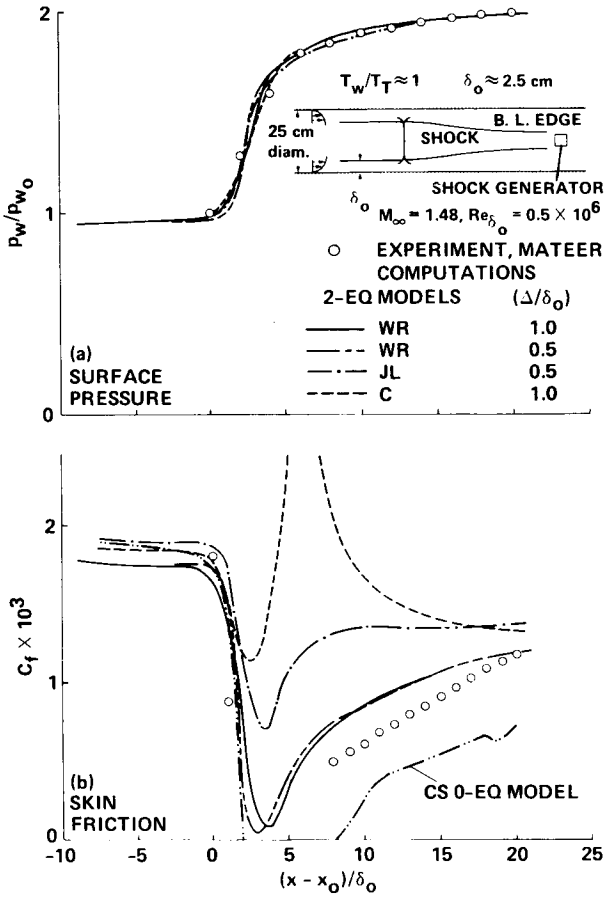

Fig. 4 Distribution of surface properties in the vicinity of normal shock wave-computations with integration to the wall.

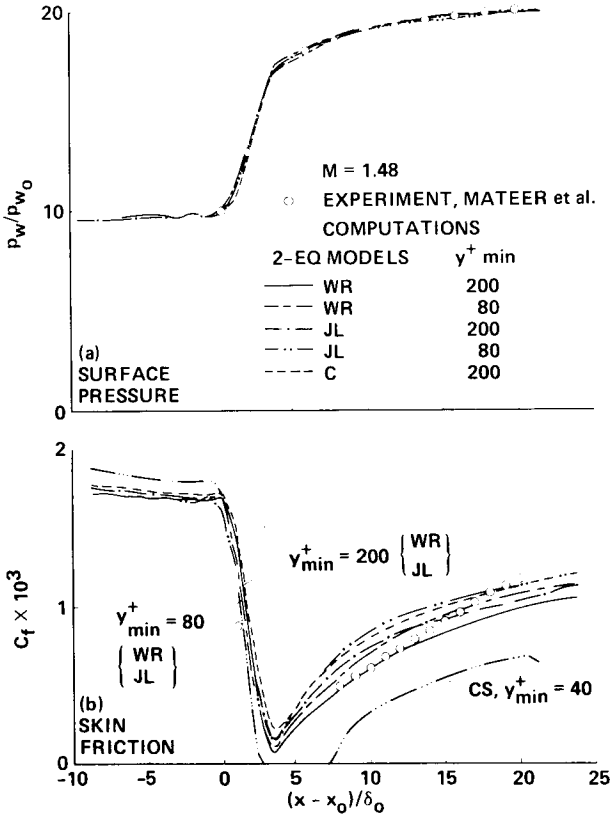

Fig. 5 Distribution of surface properties in the vicinity of normal shock wave-computations with wall functions.

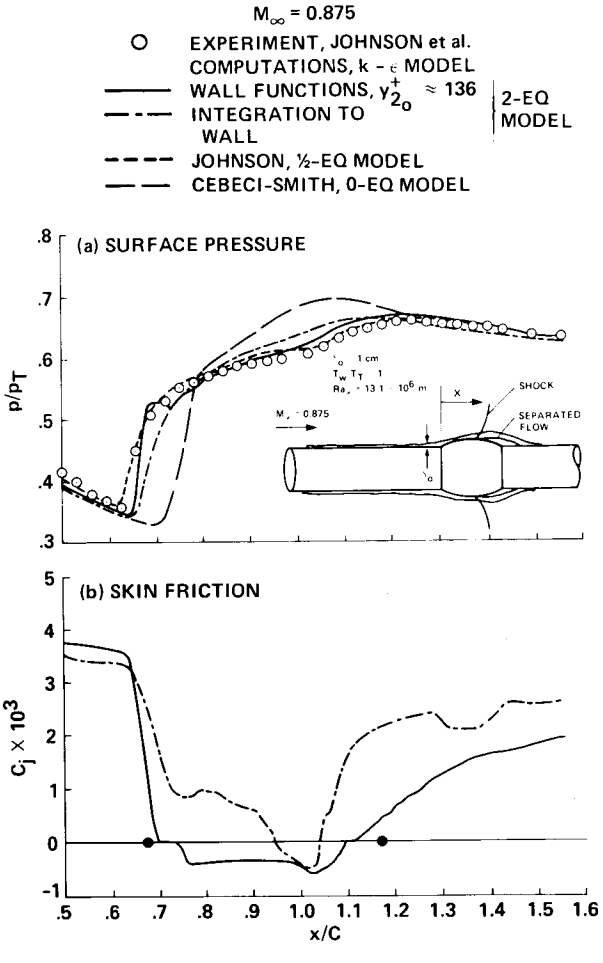

Fig. 6 Distribution of surface properties on an axisymmetric bump in transonic flow.

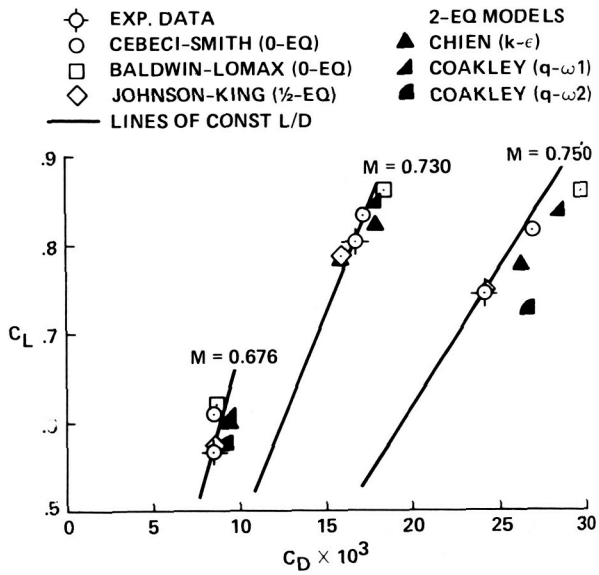

Fig. 7 Lift-drag relationships for an RAE 2822 airfoil.

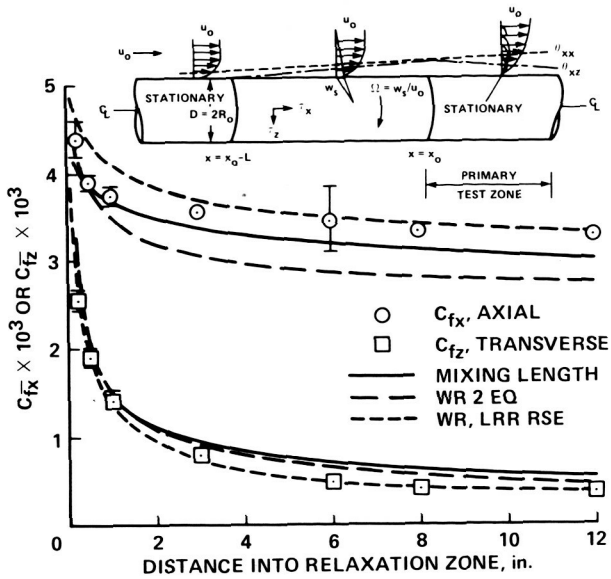

Fig. 8 Skin friction in the relaxation zone downstream of transversely sheared boundary layer.

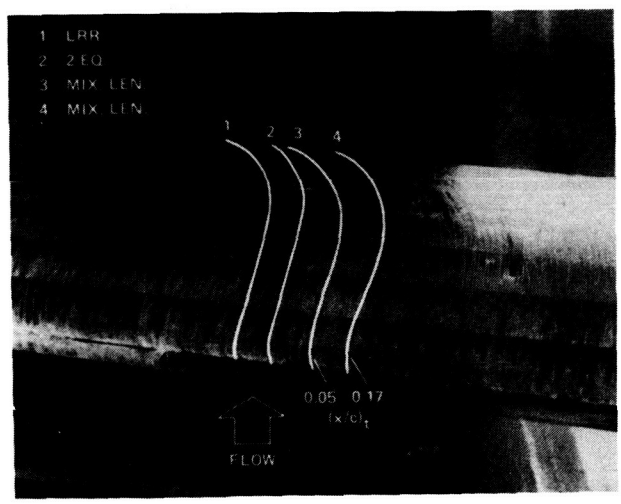

Fig. 9 Comparison of experimental and computed surface flow lines on a swept, infinitely long wing-NASA 0012 at zero angle of attack.

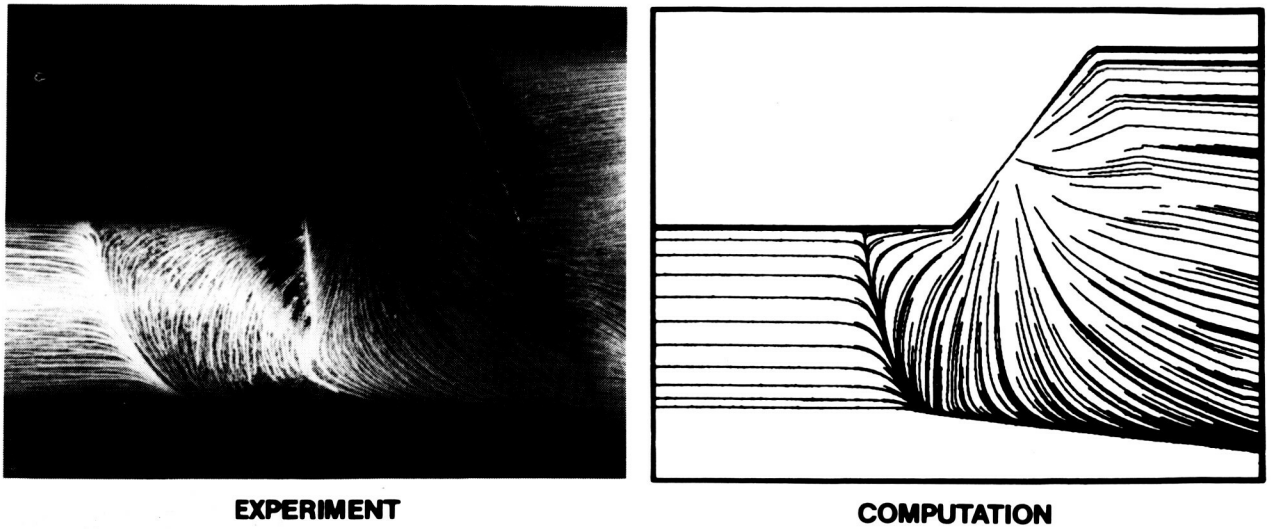

Fig. 10 Comparison of experiment and computation for a three-dimensional shock wave, turbulent boundary layer interaction.

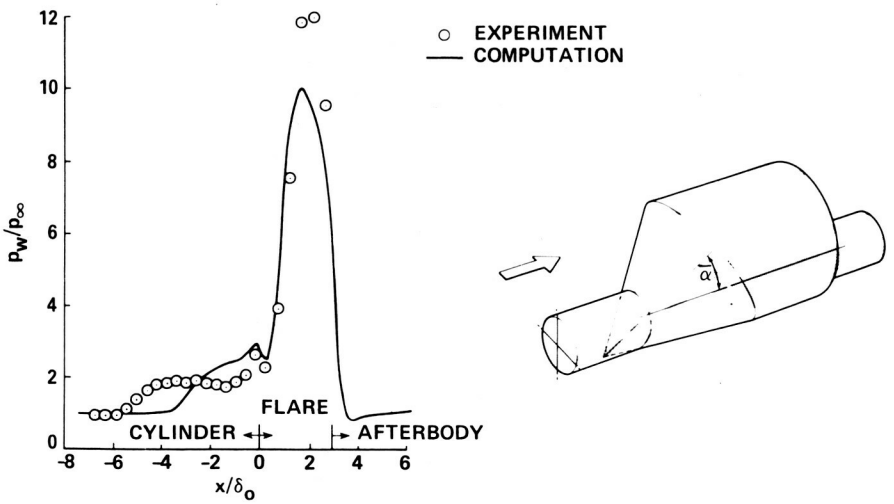

Fig. 11 Surface pressure distribution on the upwind ray of a skewed flare.